

岩手医科大学
審査学位論文
(博士)

Platelet demand modulates the type of intravascular protrusion from megakaryocytes in the mice bone marrow

Shugo Kowata,¹ Sumio Isogai,² Kazunori Murai,¹ Shigeki Ito,¹ Koujiro Tohyama,³ Masatsugu Ema,⁴ Jiro Hitomi,² and Yoji Ishida¹

¹Hematology and Oncology, Internal Medicine, Iwate Medical University School of Medicine, 19-1 Uchimaru, Morioka, Iwate 020-8505, Japan

²Anatomy and Human Embryology, Iwate Medical University School of Medicine, 2-1-1, Nishi-tokuta, Yahaba-chou, Shiwa-gun, Iwate 028-3694, Japan

³Center for Electron Microscopy and Bio-Imaging Research, Iwate Medical University School of Medicine, 2-1-1, Nishi-tokuta, Yahaba-chou, Shiwa-gun, Iwate 028-3694, Japan

⁴Research Center for Animal Life Science, Shiga University for Medical Sciences, Seta, Tsukinowa-tyo, Ohtsu, Shiga 520-2192, Japan

Corresponding author: Yoji Ishida, Hematology and Oncology, Internal Medicine, Iwate Medical University School of Medicine, 19-1 Uchimaru, Morioka, Iwate 020-8505, Japan

Tel: +81-19-651-5111, Fax: +81-19-651-5185

E-mail: yishida@iwate-med.ac.jp

Running title: visualizing platelet progenitor production within bone marrow

Financial support: This study was financially supported by a grant from the Japan Society for the Promotion of Science (Japan) 2013-2 5 4 6 1 4 5 8

Abstract

Megakaryocytes (MKs) generate platelets via intravascular protrusion termed proplatelet, which have a tandem array of platelet-sized swelling with beaded appearance. However, it remains unclear whether all intravascular protrusions translate into PP and whether MKs generate platelets without proplatelet formation. We visualized the sequential phases of intravascular protrusions and fragments in living mice bone marrow (BM) using intravital microscopy, and examined their ultrastructure. Forming intravascular protrusions were observed as highly dynamic process in which their size and shape subsequently changed to release platelet progenitors. Among these intravascular protrusions, immature thick protrusions were distinguished from proplatelets by their size and dynamic morphogenesis in time-lapse observation. In ultrastructure analysis, the thick protrusions and their fragments were characterized by a peripheral zone, abundant endoplasmic reticulum and demarcation membrane system, and random microtubule array. Proplatelets were predominant among BM sinusoid in physiological state. However, during acute thrombocytopenic period, thick protrusion increased remarkably in sinusoid. These results strongly suggests that BM MKs form and release two types of platelet progenitor via distinct intravascular protrusion, and platelet demand modulates the type of intravascular protrusion in vivo.

Key wards: Megakaryocytes, Thrombopoiesis, proplatelet, thick protrusion

Introduction

Nearly 1×10^{12} platelets, whose average lifespan is typically 7–9 days, circulate in the adult human bloodstream and are involved in hemostasis, leading to blood clot formation at sites of vascular injury (1). Nevertheless, the platelet number is tightly controlled within narrow physiological ranges (2). Platelets are formed from the cytoplasm of megakaryocytes (MKs) which resides in the bone marrow (BM). Each mature MK can produce approximately 3000 platelets within BM (3). To produce platelets, MKs extend cytoplasmic protrusions, called proplatelets, into the sinusoid vessels of the bone marrow (4). On the basis of *in vitro* observations, these proplatelets can detach from the MK cytoplasm and generate platelet-size particles that are linked by thin cytoplasmic bridges, called barbell-shaped proplatelet (5, 6). Recently, preplatelet, which is anucleate discoid particle that can reversibly convert into barbell-shaped proplatelet, is identified as a new platelet progenitor present in both cultured MKs and peripheral blood (6, 7). After leaving BM sinusoid, these platelet progenitors may convert into individual platelets in the micro capillaries of the lung, the first capillary bed to be encountered (6 - 9).

However, The detailed process of platelet progenitor production from BM MKs is unclear. The platelet territory (PT) model has been developed using light and transmission electron microscope (LM and TEM, respectively), where MK cytoplasm is divided by membrane invagination, the demarcation membrane system (DMS), into future “platelet territories”, fracturing into platelets in the BM parenchyma (10 -12). However, the release process of platelets into the circulation through the sinusoid wall has not been elucidated in the PT model (10 -12). The marginal band composed of microtubule bundles has been recognized as the cytoskeletal hallmark of definitive platelets (13, 14). The researchers who proposed the PT theory have failed to detect this hallmark in the territories. In contrast, morphological studies using scanning electron microscopy (SEM) have predicted that platelets are released from MKs via a process that remodels the entire MK cytoplasm into thin and long extensions termed proplatelets, which have a tandem array of platelet-sized swellings with a beaded appearance (4, 15, 16). Cultured MKs *in vitro* successfully demonstrated the cytoskeletal hallmark, i.e., the marginal band–like structure at the distal end of the thin and long MK extensions, and advocated the proplatelet model (5, 17, 18). It was subsequently proposed that the DMS functions as a reservoir to supply a membrane element to extend the proplatelet (19, 20). These findings have led to the proplatelet theory becoming the prevalent model, where

proplatelets undergo profound rearrangement of the cytoskeletal and membrane system during morphogenesis.

Curiously, proplatelets in BM sinusoids have been infrequently reported from LM and TEM studies of serial sections (12), although the proplatelet model was originally developed from observations of MKs in fixed specimens. It is essential to visualize the phenomena associated with proplatelet formation from MKs in intact BM. In 2007, Junt et al. captured images of MKs forming large “proplatelet-like protrusions” and routinely releasing heterogeneous large particles, but not proplatelets themselves, into sinusoids using intravital imaging (21). Although intravascular thick protrusions and fragments had been reported in early histological studies (22 -24), they had been considered as a sequential stage of proplatelet formation (19). Junt et al. concluded that these large particles might represent multiple intertwined or single immature proplatelets (21). The proplatelet, however, is originally defined as thin cytoplasm extensions into the sinusoid from MKs, forming a tandem array of platelet-sized swellings with a beaded appearance at the distal end (4, 15, 16, 19). While “proplatelet” has been applied to any intravascular protrusions from BM MKs without verification of the morphological differences between proplatelets and thick protrusions, it remains unclear whether all intravascular protrusions translate into proplatelets and whether MKs release cytoplasmic particles without proplatelet formation.

Now proplatelet theory is the unique model for explaining how MKs produce nascent platelets into the circulation. In this study, we showed that MKs used other mechanisms to permit mass production to force platelets into the blood to meet demand in an emergency.

Materials and methods

See “supplemental data” for details.

Mice

Transgenic mice expressing EGFP [EGFP-Tg mice; C57BL/6 TgN(β -act-EGFP)Osb] were kindly provided by Dr. Masaru Okabe (Genome Research Centre, Osaka University, Osaka, Japan) (25). FLK1-EGFP knock-in mice were generated as previously described (26). C57BL/6J (WT) mice (CLEA, Tokyo, Japan) were used as controls. The Institutional Animal Care and Use Committees at Iwate Medical University approved all experiments (Agreement number: 22-037).

Two-photon intravital microscopy (TPIVM) in live mice BM

EGFP-Tg mice were anesthetized and prepared for in vivo imaging as described previously (27). Mice were placed and kept for 8 h under a Zeiss LSM510 NLO microscope (Carl Zeiss, Oberkochen, Germany) using a $\times 20/1.4$ NA water objective (Olympus, Tokyo, Japan).

Fixed BM study

Mice were anesthetized and fixed by perfusion fixation method (4) by syringe pump for following examination. The BM core were immediately removed, immersed in fixative, surrounded with agar to ensure tissue integrity, post-fixed with osmium tetroxide, dehydrated, embedded in Epon. Thin coronal sections toward the central vein in the BM were examined using an electron microscope (H-7650, Hitachi, Tokyo, Japan) following uranyl acetate and lead citrate staining. For SEM, the BM were post-fixed, dehydrated, frozen, dried, mounted on metal stubs (28), and examined using SEM (Hitachi S-4700 and Nihon Denshi JSM-7001F, Tokyo, Japan). For confocal laser microscopy, the BM cores were immune-stained with rat anti-mouse glycoprotein Ib (GPIb) conjugated with DyLight-651 (Emfret Analytics, Eibelstadt, Germany) or rat anti-mouse CD41 conjugated with PE (BD Biosciences, San Jose, CA, USA) as previously described (29). The BM was visualized directly under a Zeiss LSM510 LSCM unit (Carl Zeiss).

Quantitative analysis of MK protrusions in BM sinusoids in mice

FLK1-EGFP mice were phlebotomized (15 $\mu\text{L/g}$) or intraperitoneally administrated 100 μL of 20% rabbit anti-murine platelet serum (30) in PBS. The BM cores were processed as described above for confocal laser microscopy. We counted the MKs with intravascular protrusion in each sample and distinguished them as thick protrusions or proplatelets based on the preserving peripheral zone (PZ).

Platelets and reticulated platelets in peripheral blood

Retro-orbital peripheral blood was collected. Platelet counts were measured using a Coulter Counter T540 (Coulter Electronics, Bedfordshire, England). Flow cytometric analysis of reticulated platelets was performed as described previously (31).

Statistical analysis

We used the Turkey Kramer method for statistical analysis; $P < 0.05$ was considered significant. Results are presented as the mean \pm standard deviation.

Results

Live imaging of intravascular MK protrusions

To observe the platelet formation process, we focused on MKs in the calvarium BM of EGFP-Tg mice, which were easily identified due to their giant size, round shape, nuclear lobulation, and high EGFP expression intensity [Fig. 1A (i)–(iii)]. Cytoplasmic EGFP expression was heterogeneous [Fig. 1A (iv), Movie S1].

Proplatelets

MKs budded where they were closely adhered to the sinusoid, penetrating the sinusoidal lumen. The protrusion was initially $<5\ \mu\text{m}$ wide, bulging and growing to a diameter of more than $20\ \mu\text{m}$ [mean maximum width: $13\ \mu\text{m}$ in initial proplatelet, Fig. 2B (ii-a)] with a balloon-like shape from swinging its body, as reflected by the blood flow [Fig. 1B (i), Movie S1]. The protrusion was drastically stretched by the bloodstream, resembling an airborne balloon [Fig. 1B (ii), Movies S1, S2], but remained relatively thick [mean maximum width: $6.8\ \mu\text{m}$ in transitional proplatelet, Fig. 2B (ii-b)]. Eventually, the proplatelet became elongated into a thin long shape [mean maximum width: $3.6\ \mu\text{m}$ in definitive proplatelet, Fig. 2B (ii-c)] with regional constrictions and a beaded appearance along its length [Fig. 1B (iii), Movies S2, S3]. It exhibited typical proplatelet characteristics, as demonstrated in previous reports of fixed BM and cultured MKs (9–15). The protrusion was elongated to more than $200\ \mu\text{m}$ by the bloodstream (Movie S2). It extended, resembling a string with nodular beads [Fig. 1B (iv), Movie S3]. The extremely elongated string finally snapped between the “beads” after they had stopped shifting along the string toward the tip [Fig. 1B (iv) 90 min, Movie S3]. The distal portion, resembling a short beaded string, was shed into the sinusoid [Fig. 1B (iv) 90–94 min, Movie S3]. A few minutes thereafter, the shortened proplatelet repeated the elongation in the bloodstream (Movie S4). Occasionally, a proplatelet fragment, the size of several platelets, was released into the sinusoid without apical balloon formation (Movie S5). We captured the phenomenon in which the proplatelet string was released from the distal end of the proplatelet, as suggested by previous studies (4, 5, 15, 16, 19). These results agree with the concept that proplatelets are released at distal end of proplatelet, and disagree with the notion that proplatelet elongation undergo unidirectionally as predicted by early histological studies on BM.

Blood flow had positive effects on proplatelet elongation. To evaluate the influence of hemodynamics, we measured the velocity of proplatelet elongation in BM sinusoids

in vivo using time-lapse photography and compared it with that measured under in vitro static culture conditions. The mean velocity was 17.5 $\mu\text{m}/\text{min}$ (range: 6.35–24.1 $\mu\text{m}/\text{min}$, $n = 11$) in the bloodstream, while it was 0.8 $\mu\text{m}/\text{min}$ under static culture conditions (0.41–1.25 $\mu\text{m}/\text{min}$, $n = 10$), indicating that blood flow accelerated proplatelet elongation (Fig. 1C). The balloon-like form at the apical end (mean width: 6.8 μm) and nodular beads might be advantageous for catching the blood flow. These results indicate that blood flow affects not only the shedding of the proplatelet, but also the elongation of proplatelet in vivo.

Thick protrusions

We captured 30 time-lapse images of intravascular MK protrusions using 42 EGFP-Tg mice: 84.4% were of proplatelets. However, 16.6% were of thick protrusions, differing from proplatelets in terms of shape, volume, and dynamic movement to the bloodstream (Fig. 2A, Movie S6). Thick protrusions were thick [mean maximum width: 13 μm , Fig. 2B (ii–d)], with a very large volume compared to proplatelets, and never entered elongation phases into platelet-sized beaded appearances as proplatelets did. The protrusions extended slowly to more than 100- μm lengths as their volume increased. They finally adopted a nodular or segmented shape (Fig. 2A, 0–86 min), and then snapped near where the MK penetrated into the sinusoidal lumen (Fig. 2A, 93–113 min, Movie S6).

The thicknesses of thick protrusions and proplatelets at each sequential phase were measured with time-lapse videos using TPIVM (Fig. 2B). This revealed that the thicknesses of both the thick protrusions and proplatelets were almost identical at one point. However, proplatelets became thinner, resembling the typical platelet size (mean maximal width: 3.6 μm) as the sequential phase progressed, while the thick protrusions gradually became thicker (mean maximal width: 13 μm) before being released [Fig. 2B (ii–c, d)]. Finally, proplatelets and thick protrusions released different-sized cytoplasm as the platelet progenitors into the sinusoids. SEM showed that proplatelets and thick protrusions were clearly distinguishable based on thickness and appearance (Fig. 2C).

These results indicate that BM MKs release mature platelet progenitors via proplatelet and large progenitors with unknown structural phenotype via thick protrusion. The previous histological studies on BM have been based on the notion that BM MKs must release almost structurally identical to mature platelet including proplatelet. This led us to re-examine all intravascular protrusions and their progeny from the mother MKs in detail.

Characterization of intracellular structure in mature MKs

Mature MKs are characterized by the presence of a perinuclear zone (NZ) that contains organelles, an intermediate zone (IZ) containing a well-developed DMS with defined PT, and a PZ devoid of organelles and DMS (32) [Fig. 3A (i)]. In the DMS, each PT is bound by membranes containing cytoplasm and several specific granules, mitochondria, and endoplasmic reticulum, closely resembling mature platelets [Fig. 3A (ii)] (32). TEM and SEM showed that PZ with a rugged surface and spiny projections spanned the entire IZ in mature MKs [Fig. 3A (i–iii)]. As MKs matured, DMS developed and demarcated each PT visibly [Fig. 3A (iv, v)]. The granular and mitochondrial accumulations extended towards the cell membrane, encroaching on the PZ, and finally the DMS was distributed throughout the entire cytoplasm [Fig. 3A (iv–vi)]. Thus, fully mature MKs were characterized by the presence of NZ and IZ, but had no or scant PZ [Fig. 3A (iv–vi)].

GPIb/IX/V complex identifies a membrane-structuring element (33, 34). We performed GPIb staining of the BM of EGFP -Tg (Fig. 3B) and FLK-1 EGFP Tg mice (Fig. 3C). In mature MKs [Fig. 3B (i), 3C (ii)], GPIb expression was strongly positive in the IZ, identical to the DMS, and positive in the outer PZ surface, but negative in the NZ and the inner PZ surface. This suggests that characteristic GPIb distribution distinguishes the PZ from IZ in BM MKs based on GPIb BM staining.

Intracellular structure in thick protrusions and their fragments

SEM and TEM revealed that the thick protrusions and their fragments consisted of the PZ and IZ derived from mature MKs (Fig. 4A, 4B, 4C). They had highly rugged surfaces with spiny projections throughout their entire lengths, as seen in mature MKs [Fig. 3A (i–iii)]. Peripherally, their cytoplasm was devoid of the specific granules, mitochondria, endoplasmic reticulum, and demarcation membranes, but the medulla was occupied by cytoplasm that closely resembled the IZ of mother MKs [Fig. 4A (ii, iv, v), 4B (ii, iv, v), 4C (ii–vi)]. The thick protrusions [Fig. 4A (iii)] and their fragments [Fig. 4B (iii), 4C (i)] exhibited GPIb expression patterns that corresponded to the IZ and PZ of mature MKs, i.e., GPIb expression was strongly positive in the IZ and positive in the outer PZ surface, but was negative in the inner PZ surface. As shown by TEM [Fig. 4A (iv), 4B (ii, iv, v)] and time-lapse video (Movie S6, Fig. 2A), the thick protrusions released fragments (mean maximum diameter: 13 μ m) into the sinusoids. It is known that mature platelets lose the rough endoplasmic reticulum containing ribosomes in the cytoplasm (35), but the PT of the fragments retained the endoplasmic reticulum ribosomes [Fig. 4C (iii)]. The marginal circular band composed of

microtubule bundles is the cytoskeletal hallmark of definitive platelets (13, 14). They were randomly organized in mature MKs, thick protrusions, and fragments [Fig. 4C (v, vi)]. Observing the ribosomes in the PT and microtubules that did not form marginal bands in the PZ, we concluded that the fragments do not achieve mature status to form functional platelets.

Intracellular structure in proplatelets

Figure 2B shows that initial proplatelets and thick protrusions were of almost identical thickness [Fig. 2B (ii-a, d)], but the former had scant or no PZ because the entire PZ cytoplasm had been distributed by the DMS in the mature mother MKs [Fig. 3A (iv–vi)]. The apical swelling was filled with PT and DMS [Fig. 5A (i–iii)]. Our time-lapse videos captured the transitional proplatelet with an apical balloon-like swelling (width: 2–13 μm) in the sinusoid [Movie S2, Fig. 1B (ii)]. The transitional proplatelet was thicker than the typical proplatelet (width: 1–7 μm) and the cytoplasm exhibited the reticular expression pattern of GPIb [Fig. 5B (iii)]. As shown by GPIb expression (Fig. 5B (iii)) and TEM [Fig. 5B (iv, v)], the transitional proplatelet was characterized by the lack of PZ and segmented surface, which represented fracturing PT. The cytoplasm of the transitional proplatelet contained specific granules, mitochondria, endoplasmic reticulum, and demarcation membranes, exhibiting the same features as fully mature MKs [Fig. 5B (v)]. The microtubules were concentrated and ran longitudinally to the long axis within the constriction zone [red arrows, Fig. 5B (v)].

In the definitive phase, the transitional proplatelet was transformed into the proplatelet from which platelet progeny were released as a short beaded string [Movie S3, Fig. 1A (iii, iv)]. The proplatelet was a long thin projection with a smooth surface and was devoid of PZ (Fig. 5C). At the attenuating process from the transitional proplatelet, the beaded cytoplasm of the proplatelet greatly resembled to that of a single platelet and the microtubules ran longitudinally to the long axis of the beaded cytoplasm [Fig. 5C (v)]. In the platelet progenitor (proplatelet released into the sinusoid), the microtubules ran parallel to the long axis of the progenitor and formed bundles to generate the marginal band [Fig. 5D (ii)]. These results indicate that proplatelets release mature platelet progenitors which are almost structurally identical to mature platelet, but thick protrusions release immature platelet progenitors which are almost identically to mother MKs.

Dominance of thick protrusions in thrombocytopenia with high thrombopoietic activity

In acute blood loss, platelet production may increase 6–20-fold to increase their numbers (3), but not all platelets in the peripheral blood are of uniform size, density, and activity (36). There had been reported that the proportion (but not absolute number) of beaded proplatelets in the circulation increased 3-fold 24 h after acute thrombocytopenia was induced (37). In our time-lapse images, 84.4% and 16.6% of the images from the 42 EGFP Tg mice were proplatelets and thick protrusions, respectively.

To evaluate how thick protrusions reacted to acute thrombocytopenia, we quantified the proportions of proplatelets and thick protrusions in BM sinusoid of acute thrombocytopenic mice. We used FLK-1 EGFP Tg mice and GPIb staining of fixed BM sample to identify the sinusoidal endothelial cells and types of intravascular protrusions, as shown in Fig.3-5. Forty-eight hours after phlebotomy, the platelet count decreased to approximately 75% of the values in untreated mice (Fig. 6A). At 72 hours, the platelet count recovered to above normal levels and remained for up to 168 hours. At 48 h after phlebotomy, the frequency of reticulated platelets increased to 7.8-fold (control: 1.0% \pm 0.1%, 48 h: 7.84% \pm 2.0%, $P < 0.01$), suggesting that immature platelets were released in abundant numbers into the circulation. In the BM sinusoids, the frequency of thick protrusions significantly increased to 5.2–6.3 times at 24 and 48 h after phlebotomy, respectively (control: 10.8% \pm 10.1%, 24 h: 56.4% \pm 16.2% ($P < 0.05$), 48 h: 68.9% \pm 0.7% ($P < 0.05$)). As the platelet count recovered to the normal level at 72 h after phlebotomy, the frequency of thick protrusions decreased drastically to below normal levels.

In mice treated with anti-platelet serum, the platelet count dropped to approximately 10% of the untreated value in venous blood at 24 h after injection (Fig. 6B). The platelet count recovered significantly to normal level by 72 h and continued to increase up to 168 h. At 24 and 48 h after treatment, the frequency of reticulated platelets had increased 10-15-fold (control: 1.0% \pm 0.1%, 24h: 15.6% \pm 5.2% ($P < 0.05$), 48 h: 10.4% \pm 4.4% ($P < 0.05$)). Similar to the phlebotomized mice, the frequency of thick protrusions in the BM sinusoids was significantly increased by 4.8 times at 48 h after treatment (control: 15.6% \pm 14.5 %, 48 h: 75.5% \pm 3.3% ($P < 0.05$)). While the platelet count recovered at 72 h, the frequency of thick protrusions decreased drastically. The frequency of thick protrusions fluctuated with that of reticulated platelets in both phlebotomized and anti-platelet serum-treated mice.

The findings from acute thrombocytopenic mice showed a clearly inverse correlation in dominance between proplatelets and thick protrusions and strongly suggest that platelet demand directly modulates the type of intravascular MK protrusion in the BM.

Discussion

In this study, we reported the detailed process in platelet progenitor formation by BM MKs. Our analysis revealed the first presentation of dynamic aspects of this process *in vivo*. The detailed analysis from TPIVM clearly demonstrated the dynamic BM MK produces a single typical proplatelet in the sinusoid. In addition, MK released large cytoplasmic fragment without proplatelet and preplatelet formation.

The proplatelet formation initiated with sending small protrusions into the sinusoid through endothelial wall. Small protrusions gradually became larger spherical shape in the blood stream. This process appeared to be that MKs took great efforts to send the essential elements of nascent platelet into vessel lumen via narrow entrance of endothelial pore before beginning of elongation. The initial proplatelet then drastically changed into transitional proplatelet with elongating and becoming thinner. The transitional proplatelet gradually changed into long, thin, and beaded protrusions, named as definitive proplatelet, which were more than 200- μm long into the sinusoid, consistent with the typical proplatelet characteristics reported previously (4, 15, 16). Blood flow accelerated the proplatelet elongation, suggesting that the shape of initial proplatelet have been advantageous for catching the blood flow. Finally, the distal portion of the proplatelet was released into the sinusoidal blood as a short string with a beaded appearance.

In ultra-structural analysis, we found a thicker (width: 2-13 μm) transitional proplatelet with a segmented surface, representing the fracturing DMS and PT. The transitional proplatelet was often converted into the proplatelet at the distal region. The microtubules were randomly organized in the residual PT, whereas they were running parallel to the long axis within the constricted region. In the fragment of proplatelets, a bundle of microtubules were formed within their cytoplasm, as seen in preplatelets from cultured MK (38) and circulating platelets (13, 14). These data are consistent with that bundle of microtubule organization during proplatelet and preplatelet formation *in vitro* (5, 6), and strongly suggests that nascent platelet is formed at the distal region of proplatelets *in vivo*.

In vitro, proplatelet showed complex and bifurcated morphology and often entangled each other, while long proplatelets with rarely branching were found in BM sinusoid (Fig 1B, 5B-D). Thus, we interpret the complex bifurcated proplatelet as unique morphogenesis only observed in static culture condition *in vitro*, and as a phenomenon which reflects the ability to change with proplatelet fragment to individual mature platelet in the shear flow after leaving BM.

We captured 30 time-lapse images, of which 25 (84.4%) were of the proplatelet. Five images (16.6%) were of thick protrusions. They did not undergo elongation into the platelet-sized beaded appearance as the proplatelet did. In ultra-structural analysis, the thick protrusions and large fragments possessed the same rugged PZ surface surrounding the abundant DMS and territories. We also confirmed that daughter thick protrusions or fragments held the same status for specific granules, organelles, rough endoplasmic reticulum, and randomly organized microtubules as seen in the cytoplasm of mother MKs. These immature phenotype suggested that the fragments contained the elements of nascent platelet, but had not achieved the mature status of microtubule array as seen in the proplatelet (5, 17 -19) and preplatelet (6, 7).

Our dynamic and structural analyses of intravascular protrusions in BM strongly suggest that BM MKs occasionally form and release platelet progenitors into sinusoid without proplatelet formation. Previous studies has been based on the notion that nascent platelets, which are almost identical to mature circulating platelets in size and structure, must be released from BM MKs. This notion has been supported by the proplatelet model (4, 5, 15, 16, 19, 38), and has been inconsistent with the appearance of large cytoplasmic fragments in BM sinusoid (22, 23, 24) and pulmonary capillary (9, 39, 40). The previous studies using intravital microscopy (21, 41) did not reveal the sequential changes in the size of intravascular protrusions during the entire process. The authors might have believed that the thick protrusions represented intertwined or immature proplatelets as a sequential stage of proplatelet formation, in line with a concept from proplatelet model (19, 21).

The data obtained from acute thrombocytopenic mice with phlebotomy or anti-platelet serum administration clearly showed the abundant increase of young platelets in the peripheral blood and the inverse correlation in the dominancy between proplatelets and thick protrusions within BM vessels, suggesting that thick protrusions may be greatly advantageous for supplying immature platelets into the vessel lumen to satisfy the demand for new platelets rapidly.

Our observation of large fragments in sinusoid explains how to form platelet progenitors. Large MK fragment preserving PZ covering the PT and DMS, also called giant platelet, have been frequently observed in venous blood in reactive thrombocytosis or chronic idiopathic thrombocytopenic purpura (32). Fragmented proplatelets, barbell-shaped platelets, and preplatelet have been frequently observed in the venous blood (6, 7, 9, 42). The preplatelet is considered as the intermediate structure between the proplatelet and platelet because it is a large anuclear disc (diameter: 2–10 μm) with a thick cortical microtubule coil and retains the capacity to reversibly convert

into a barbell-shaped proplatelet (6, 7). In these platelets and their progenitors, the marginal band has been identified in platelets and preplatelets, but not in giant platelets (32). Interestingly, thick protrusion and large fragment preserved abundant rough endoplasmic reticulum (Fig. 4), while circulating platelets usually have lost them. In addition, thick protrusion from MK in vitro was divided into large fragments, and eventually became proplatelet (data not shown). These data suggest that large fragment is the most premature platelet progenitor from BM MK, and may translate into mature platelets via proplatelet and preplatelet in the blood stream after leaving BM.

There have been many reports that the lung is the primary platelet production site (43). We found that entire MK (Fig. 3) and exhausted MKs were carried away by the bloodstream from the BM (data not shown), consisted with previous reports (9, 40). These data support the hypothesis that the pulmonary capillary is the secondary site of platelet production, where MKs generate platelet progenitors, and platelet progenitors translate into individual platelets.

Thrombopoietin (TPO) acts as the major regulator that promotes the growth and development of MKs from precursor cells (1). In clinical setting, TPO mimetics are highly effective in raising the platelet count in patients with immune thrombocytopenic purpura (44). However, the serum TPO level is not increased significantly in immune thrombocytopenia with the presence of MKs in BM (45), and is mainly regulated by MK mass rather than platelet mass (46). In addition, TPO is not a direct stimulator of proplatelet formation in human (47) and mice MKs (48), and acts as a negative regulator of proplatelet formation via Rho/ Rock pathway (49). These data suggest that, although TPO is one key driver of MK differentiation and maturation, there may be other factors which initiate and regulate the process of platelet progenitors formation on mature MKs.

In conclusion, mature MKs devoid of PZ generate transitional proplatelets and then definitive proplatelets into the sinusoidal lumen, and release the progeny in preplatelet-like form into the sinusoidal blood. Mature MKs with a thick PZ generate thick protrusions into the sinusoidal lumen, and release their progeny in giant platelet-like form into the sinusoidal blood. Blood flow accelerates elongation of intravascular protrusions, detachment, and move of platelet progenitors. After leaving BM, these platelet progenitors eventually change into individual platelets (Fig. 7). Proplatelets are formed predominantly in physiological state. However, thick protrusion are formed predominantly in acute supply of platelet mass. Thus, platelet demand directly modulates the type of intravascular protrusion from MKs in the BM.

Further studies are needed to elucidate whether these structural heterogeneity of platelets and their progenitors in circulating blood influence the pathology of platelet related diseases including arteriosclerosis, thrombosis, innate immune response, and cancer metastasis.

Acknowledgements

The authors thank Yukie Takahashi for BM processing, Hiroko Chiba and Sizune Hirayama for technical assistance in animal processing, Kuniaki Sasaki for technical assistance in SEM observation, and Yasuhiko Tsukushi and Tatsuo Oyake for critical review of the manuscript.

Authorship Contributions

S.K. designed, performed, analyzed, and interpreted all experiments and results and wrote the paper; S.I. designed and performed the TPIVM and analyzed and interpreted the results; K.M. and Sigeki I. performed the in vitro proplatelet assay and immunofluorescence staining; K.T. designed and performed the electron microscopy experiments; M.E. generated the FLK1–EGFP mice; J.H. interpreted the TPIVM results; Y.I. is the corresponding author, designed the experiments, interpreted the results, formulated the discussion, and assisted in manuscript preparation and editing.

Conflict of interest disclosure

The authors declare no competing financial interests.

Please address correspondence to Y.I. (yishida@iwate-med.ac.jp).

References

1. Kaushansky K. Determinants of platelet number and regulation of thrombopoiesis. *Hematology Am Soc Hematol Educ Program*. 2009;147–152.
2. Aster RH. Pooling of platelets in the spleen: role in the pathogenesis of “hypersplenic” thrombocytopenia. *J Clin Invest*. 1966;45:645–657.
3. Harker LA, Finch CA. Thrombokinetics in man. *J Clin Invest*. 1969;48:963–974.
4. Becker RP, De Bruyn PP. The transmural passage of blood cells into myeloid sinusoids and the entry of platelets into the sinusoidal circulation; a scanning electron microscopic investigation. *Am J Anat*. 1976;145:183–205.
5. Italiano JE Jr, Lecine P, Shivdasani RA, et al. Blood platelets are assembled principally at the ends of proplatelet processes produced by differentiated megakaryocytes. *J Cell Biol*. 1999;147:1299–1312.
6. Thon JN, Montalvo A, Patel-Hett S, et al. Cytoskeletal mechanics of proplatelet maturation and platelet release. *J Cell Biol*. 2010;191:861–874.
7. Thon JN, Macleod H, Begonja AJ, et al. Microtubule and cortical forces determine platelet size during vascular platelet production. *Nat Commun*. 2012;3:852.
8. Handagama PJ, Feldman BF, Jain NC, et al. Circulating proplatelets: isolation and quantitation in healthy rats and in rats with induced acute blood loss. *Am J Vet Res*. 1987;48:962-5.
9. Zucker-Franklin D, Philipp CS. Platelet production in the pulmonary capillary bed: new ultrastructural evidence for an old concept. *Am J Pathol*. 2000;157:69–74.
10. Yamada E. The fine structure of the megakaryocyte in the mouse spleen. *Acta Anat (Basel)* 1957;29:267–290.
11. Behnke O. An electron microscope study of the rat megakaryocyte. II. Some aspects of platelet release and microtubules. *J Ultrastruct Res*. 1969;26:111–129.
12. Kosaki G. In vivo platelet production from mature megakaryocytes: does platelet release occur via proplatelets? *Int J Hematol*. 2005;81:208–219.
13. Behnke O. Microtubules in disk-shaped blood cells. *Int Rev Exp Pathol*. 1970;9:1-92.
14. White JG, Rao GH. Microtubule coils versus the surface membrane cytoskeleton in maintenance and restoration of platelet discoid shape. *Am J Pathol*. 1998;152:597–609.
15. Radley JM, Scurfield G. The mechanism of platelet release. *Blood*. 1980;56:996–999.
16. Muto M. A scanning and transmission electron microscopic study on rat bone marrow sinuses and transmural migration of blood cells. *Arch Histol Jpn*. 1976;39:51–66.

17. Richardson JL, Shivdasani RA, Boers C, et al. Mechanisms of organelle transport and capture along proplatelets during platelet production. *Blood*. 2005;106:4066-75.
18. Patel SR et al. Differential roles of microtubule assembly and sliding in proplatelet formation by megakaryocytes. *Blood*. 2005;106:4076–4085.
19. Radley JM, Haller CJ. The demarcation membrane system of the megakaryocyte: a misnomer? *Blood*. 1982;60:213–219.
20. Schulze H, Korpál M, Hurov J, et al. Characterization of the megakaryocyte demarcation membrane system and its role in thrombopoiesis. *Blood*. 2006;107:3868-75
21. Junt T, Schulze H, Chen Z, et al. Dynamic visualization of thrombopoiesis within bone marrow. *Science*. 2007;317:1767-70 .
22. Wright JH. Die Entstehung der Blutplättchen. *Virchows Arch*. 1906;186:55–63.
23. Breton-Gorius J, Reyes F. Ultrastructure of human bone marrow cell maturation. *Int Rev Cytol*. 1976;46:251–321.
24. Lichtman MA, Chamberlain JK, Simon W, et al. The parasinusoidal location of megakaryocytes in marrow: a determinant of platelet release and a physiologic version of vascular invasion and metastasis. *Trans Assoc Am Physicians*. 1977;90:313–323.
25. Okabe M, Ikawa M, Kominami K, et al. 'Green mice' as a source of ubiquitous green cells. *FEBS Lett*. 1997;407:313–319.
26. Ema M, Takahashi S, Rossant J. Deletion of the selection cassette, but not cis-acting elements, in targeted Flk1-lacZ allele reveals Flk1 expression in multipotent mesodermal progenitors. *Blood*. 2006;107:111–117.
27. Lo Celso C, Lin CP, Scadden DT. In vivo imaging of transplanted hematopoietic stem and progenitor cells in mouse calvarium bone marrow. *Nat Protoc*. 2011;6:1–14.
28. Isogai S, Horiguchi M, Hitomi J. The para-aortic ridge plays a key role in the formation of the renal, adrenal and gonadal vascular systems. *J Anat*. 2010;216:656-70.
29. Takaku T, Malide D, Young NS, et al. Hematopoiesis in 3 dimensions: human and murine bone marrow architecture visualized by confocal microscopy. *Blood*. 2010; 116:41-45
30. Levin J, Levin FC, Metcalf D. The effects of acute thrombocytopenia on megakaryocyte-CFC and granulocyte-macrophage-CFC in mice: studies of bone marrow and spleen. *Blood*. 1980;56:274-83.
31. Kienast J, Schmitz G. Flow cytometric analysis of thiazole orange uptake by platelets: a diagnostic aid in the evaluation of thrombocytopenic disorders. *Blood*. 1990;75:116–121.
32. Zucker-Franklin D. Megakaryocyte and platelet structure in thrombocytopoiesis: the effect of cytokines. *Stem Cells*. 1996;14 Suppl 1:1–17.

33. White JG, Krumwiede MD, Escolar G. Glycoprotein Ib is homogeneously distributed on external and internal membranes of resting platelets. *Am J Pathol.* 1999;155:2127–2134.
34. Strassel C, Eckly A, Léon C, et al. Intrinsic impaired proplatelet formation and microtubule coil assembly of megakaryocytes in a mouse model of Bernard-Soulier syndrome. *Haematologica.* 2009;94:800–810.
35. White JG. Platelet structure. *Platelets*, third edition. 2013:117–144. Elsevier, Oxford, UK.
36. Leader A, Pereg D, Lishner M. Are platelet volume indices of clinical use? A multidisciplinary review. *Ann Med.* 2012;44:805–816.
37. Tong M, Seth P, Penington DG. Proplatelets and stress platelets. *Blood.* 1987;69:522–528.
38. Radley JM, Hartshorn MA. Megakaryocyte fragments and the microtubule coil. *Blood Cells.* 1987;12:603–614.
39. Ascoff L. Ueber capillare Embolie von riesenkernhaltigen Zellen. *Arch Pathol Anat Phys.* 1893;134:11–14.
40. Levine RF, Eldor A, Shoff PK, et al. Circulating megakaryocytes: delivery of large numbers of intact, mature megakaryocytes to the lungs. *Eur J Haematol.* 1993;51:233–246.
41. Zhang L, Orban M, Lorenz M, et al. A novel role of sphingosine 1-phosphate receptor S1pr1 in mouse thrombopoiesis. *J Exp Med.* 2012;209:2165–2181.
42. Behnke O, Forer A. From megakaryocytes to platelets: platelet morphogenesis takes place in the bloodstream. *Eur J Haematol.* 1998;61:3–23.
43. Weyrich AS, Zimmerman GA. Platelets in lung biology. *Annu Rev Physiol.* 2013;75:569–591.
44. Kuter DJ, Bussel JB, Lyons RM, et al. Efficacy of romiplostim in patients with chronic immune thrombocytopenic purpura: a double-blind randomised controlled trial. *Lancet.* 2008;371:395–403.
45. Emmons RV, Reid DM, Cohen RL, et al. Human thrombopoietin levels are high when thrombocytopenia is due to megakaryocyte deficiency and low when due to increased platelet destruction. *Blood.* 1996;87:4068–71.
46. Nagasawa T, Hasegawa Y, Shimizu S, et al. Serum thrombopoietin level is mainly regulated by megakaryocyte mass rather than platelet mass in human subjects. *Br J Haematol.* 1998;101:242–4.
47. Ito T, Ishida Y, Kashiwagi R, et al. Recombinant human c-Mpl ligand is not a direct stimulator of proplatelet formation in mature human megakaryocytes. *Br J*

Haematol. 1996;94:387-90.

48. Ishida Y, Ito T, Kuriya S. Effects of c-mpl ligand on cytoplasmic maturation of murine megakaryocytes and on platelet production. *J Histochem Cytochem.* 1998;46:49-57.

49. Chang Y, Auradé F, Larbret F, et al. Proplatelet formation is regulated by the Rho/ROCK pathway. *Blood.* 2007;109:4229-36.

Figure legends

Figure 1.

(A) MKs in the skull BM of EGFP-Tg mouse. (i) MKs located close to the BM sinusoid of the skull (Giemsa-stained) from which we captured the live images (inset). (ii) Mature MKs are clearly identified by their large size ($>20\ \mu\text{m}$) and reddish or yellowish color in the section stained with anti-CD41 antibody (red). (iii) Live image of BM MKs from TPIVM. The parenchyma was filled with EGFP-positive cells, except the sinusoid, which is dark because mature erythrocytes are EGFP-negative. MKs are easily recognizable along the sinusoid. (iv) Live image of mature MKs from TPIVM demonstrating heterogeneous EGFP expression. S: Sinusoid, white arrow: MK. Scale bar: $10\ \mu\text{m}$ in all panels. **(B) Sequential phases of proplatelet formation captured by TPIVM** (Supplemental Movies 1–3). (i) Initial phase of proplatelet (Supplemental Movie 1): A tiny protrusion begins to penetrate the sinusoidal wall (210), swelling into an elliptical shape. (ii) Transitional phase of proplatelet (Supplemental Movie 2): The apical swelling caught up in the blood flow. The relatively thick proplatelet is stretched by the bloodstream. (iii) Definitive phase of proplatelet (Supplemental Movie 3): With the elongation of the transitional proplatelet, the string between the beads gradually becomes thinner. The interval between the beads (colored dots) stretches and each bead shifts toward the tip in the apical region of proplatelet. (iv) Release of fragment into blood (Supplemental Movie 3): At the proplatelet apical region, the thin string between the beads snaps (white arrowheads) and a short fragment is released into the blood (iv - 90). MK: Megakaryocyte, S: sinusoidal lumen; numerals represent elapsed time (minutes). A white line delineates the sinusoidal lumen. A white arrow indicates the direction of the blood flow. Red arrowheads indicate the proplatelet. Scale bar: $10\ \mu\text{m}$. **(C) Comparison of proplatelet elongation velocity in vivo and in vitro.** Velocity was calculated using TPIVM time-lapse videos of intact BM MKs in vivo and MKs cultured in suspension harvested in vitro from EGFP-Tg mice. Mean velocity of proplatelet elongation from intact MKs in the bloodstream is $17.5\ \mu\text{m}/\text{min}$ (range: $6.35\text{--}24.1$, $n = 11$). That from MKs in static culture condition is $0.8\ \mu\text{m}/\text{min}$ (range: $0.41\text{--}1.25$, $n = 10$).

Figure 2.

(A) Sequential phases of thick protrusion captured by TPIVM (Supplemental Movie 6). The protrusion begins to invade into the sinusoidal lumen (0) and emerges gradually as sequential thick masses (3-61). As its volume increases, the thick protrusion is greatly influenced by the bloodstream, eventually detaching at the root (white arrowheads) and being released into the blood as sequential thick masses (113). Numerals represent

elapsed time (minutes). A white line delineates the sinusoidal lumen. A white arrow indicates the direction of blood flow. Red arrowheads indicate the protrusion. Scale bar: 5 μm . **(B) Thickness of intravascular protrusions.** (i) Schematic drawings of the proplatelet formation process (top) and thick protrusion (bottom). The thickest part of the proplatelet in the sequential phases (a–c) and the thick protrusion (d) were measured with time-lapse videos using TPIVM. The sinusoidal wall is colored red. (ii) a: Width of initial proplatelet (mean: 13.2 μm , n = 12), b: width of transitional proplatelet (mean: 6.9 μm , n = 24), c: width of definitive proplatelet (mean: 3.6 μm , n = 25), d: width of thick protrusion (mean: 13.0 μm , n = 5). **(C) SEM image of proplatelet and thick protrusion within a BM sinusoid in the skull.** (i) The thin proplatelet (white arrows) has a smooth surface; the thick protrusion (red arrows) is covered by a PZ with a rugged surface with spiny projections (white arrowheads). Note the close-up view of a cracked section of the proplatelet (ii) and thick protrusion (iii) in the inset in (i). The medulla of the thick protrusion contains a DMS and PT (red arrowheads). Scale bar: 5 μm in (i), 1 μm in (ii) (iii).

Figure 3. Megakaryocyte.

(A) (i–iii): TEM and SEM images of mature MK. (i) TEM image of a typical mature MK characterized by PZ (double arrow), IZ, and NZ. (ii) Magnified image of inset in (i). Note the rugged surface (black arrows) with spiny projections (arrowhead) on the outer PZ surface devoid of organelles and DMS. PT containing specific granules, mitochondria, and endoplasmic reticulum closely resembling mature platelets are demarcated by DMS in the IZ. (iii) SEM image of a cracked section showing PT demarcated by the DMS in the IZ and PZ devoid of DMS in mature MKs. The outer PZ surface of the mature MK is characterized by a rugged surface with spiny projections. (iv–vi) TEM and SEM of fully mature MK. (iv) Fully mature MK characterized by IZ and NZ but devoid of PZ because the DMS is distributed throughout the entire cytoplasm upon maturation. (v) Magnified image of inset in (A-iv). The cytoplasm is heavily perforated by the fine canaliculi of the DMS and visibly demarcated into PT. (vi) SEM of fully mature MK characterized by dominant IZ but scant PZ. Scale bar: 10 μm in (i)(iv), 1 μm in (ii-iii)(v-iv). **(B)** (i) Mature MK of EGFP-Tg (green) mouse immunostained with GPIb/IX/V (red), (ii) EGFP(green), and (iii) merged image of EGFP and GPIb staining. Mature MK is characterized by the PZ, IZ, and NZ; the PZ covers the entire area of the IZ. GPIb expression is strongly positive in the IZ (red in [i], orange in [iii]). The outer PZ surface (red layer in [i, iii]) is GPIb-positive but the inner PZ surface (green in

[ii]) is GPIIb- β -negative. Note the rugged surface (black arrows) as seen in Fig. 3A (ii). PZ: Double arrowheads, Scale bar: 5 μ m. **(C)** (i) Three-dimensionally reconstructed MKs immunostained with GPIIb β (green) and sinusoids (red) in FLK-1–EGFP Tg mouse. ii) Cross-section of mature MKs adhering to the sinusoid. The outer surface of the PZ and IZ are GPIIb β -positive, but the NZ and the inner side of the PZ are GPIIb- β -negative. PZ: Double arrowheads, Scale bar: 50 μ m in (i), 10 μ m in (ii). **(D)** MK within the BM sinusoid. Three-dimensionally reconstructed (i) and optical slice (ii) images of MK (green) within the sinusoid (red) immunostained with GPIIb β (green) in FLK-1–EGFP (red) Tg mouse. Using TPIVM, we incidentally captured the phenomenon where a whole mature MK, characterized by the presence of PZ and NZ, invaded into the sinusoid (S) and was carried away by blood flow in the BM. This histological data support the phenomena observed *in vivo*. Scale bar: 10 μ m. EC: endothelial cells. IZ: intermediate zone. MK: megakaryocyte. NZ: nuclear zone. PT: platelet territory. PZ: peripheral zone. S: sinusoid.

Figure 4. Thick protrusion and its fragment.

(A) Thick protrusion (Supplemental Movie 6 and Fig. 2A). (i) Three-dimensionally reconstructed image of thick protrusion immunostained with GPIIb β (green) emerging from the MK into the sinusoid (endothelia in red) in an FLK-1–EGFP Tg mouse. (ii) SEM image of thick protrusion. PZ with a rugged surface and spiny projections covers the IZ entirely. (iii) Optical section of thick protrusion in (i). The outer PZ surface and DMS are GPIIb β -positive but the inner PZ surface is GPIIb β -negative. PZ: Double arrowheads. (iv) TEM image of MK releasing thick protrusion and fragments into the sinusoid. PZ: Double arrowheads. (v) Magnified image of inset in (iv). PT demarcated by the DMS contain specific granules, mitochondria, endoplasmic reticulum, and ribosomes (R), resembling mature platelets in the IZ. The characteristic rugged surface (black arrows) and fine projections (black arrowheads) of the thick protrusion are devoid of organelles and DMS, but granules and organelles encroach on the inner PZ area. Scale bar: 5 μ m in (i-iv), 1 μ m in (vi). **(B) Release of fragments from thick protrusion** (Supplemental Movie 6 and Fig. 2A). (i) Three-dimensionally reconstructed image of thick protrusion (arrow) releasing its progeny (arrowhead) into the sinusoid (endothelia in red) in a FLK-1–EGFP Tg mouse immunostained with GPIIb β (green). (ii) TEM image of the PTs and DMS entirely covered by the PZ in the thick protrusion (arrow) and fragment (arrowhead). An erythrocyte is located between them. (iii) Magnified optical section of inset in (i). The outer PZ surface and DMS of the thick

protrusion and fragment are GPIIb β -positive, but the inner PZ surface is GPIIb β -negative (dark area indicated with double arrow). (iv) TEM image of thick protrusion releasing its fragment into the sinusoid and (v) close-up view of inset in (iv) depicting the fine architecture of the thick protrusion and fragment at the releasing point. The PZ is retained at both detaching ends. Scale bar: 5 μ m in (i-iv), 1 μ m in (vi). **(C) Fragment from thick protrusion.** (i) Optical section of spherical fragment immunostained with GPIIb β (green) in the sinusoid (endothelia in red) in a FLK-1-EGFP Tg mouse. GPIIb β expression is strongly positive heterogeneously in the medulla corresponding to the DMS, positive in the outer PZ surface, but negative in the inner PZ surface (double arrow). (ii) TEM image of fragment. PZ with a rugged surface (arrows) and fine projection (arrowheads) covers the PT. (iii) Magnified view of inset in (ii). TEM image depicts the ribosome on the endoplasmic reticulum (R) of the PT. (iv-vi) Sequentially magnified TEM images illustrating randomly arranged microtubules (red arrows) in the PZ of the fragment. (vi) Microtubules that have not established the circular bundle of microtubules i.e., “marginal band of platelet.” Scale bar: 1 μ m in (i-iv), 500 nm in (v,vi). DMS: demarcation membrane system. IZ: intermediate zone. MK: megakaryocyte. NZ: nuclear zone. PT: platelet territory. PZ: peripheral zone. S: sinusoid.

Figure 5. Sequential phases of proplatelet formation.

(A) Proplatelet in the initial phase (Supplemental Movie 1 and Fig. 1B-i). (i) TEM image of an apical swelling of the proplatelet protrudes into the sinusoid from the mature MK covered with scant PZ. Arrowheads indicate sinusoid endothelia. (ii) Magnified views in inset depict the root of the protrusion penetrating the sinusoidal endothelia and (iii) the apical surface facing the sinusoidal lumen. The swelling is covered with scant PZ at its root but the PT are directly exposed to the sinusoid. Scale bar: 5 μ m in (i), 1 μ m in (ii,iii). **(B) Proplatelet in the transitional phase** (Supplemental Movie 2 and Fig. 1B-ii). (i) Three-dimensionally reconstructed transitional proplatelet (asterisks and rhombus) immunostained with GPIIb β (green) in the sinusoid (endothelia in red) of a FLK-1-EGFP Tg mouse. The relatively thick proplatelet is elongated by the bloodstream within the sinusoid. (ii) SEM image of the transitional proplatelet. As shown in Figure 5A-ii, the root of transitional proplatelet (asterisk) is still covered with scant PZ characterized by a rugged surface with fine projections at the proximal region (cracked section indicated by asterisk). (iii) Magnified optical section in inset of Figure 5B-i. The transitional proplatelet (asterisk) heterogeneously expresses EGFP identically to the DMS. (iv) As seen in TEM,

transitional proplatelets (rhombus) are devoid of PZ in the sinusoid. (v) Magnified view of inset in (iv) depicting microtubules (red arrows) running parallel along the long axis of a transitional proplatelet. Scale bar: 5 μm in (i-iii), 1 μm in (iv,v). **(C) Proplatelet in the definitive phase** (Supplemental Movie 3 and Fig. 1B-iii, iv). (i) Three-dimensionally reconstructed proplatelet (asterisk and rhombus) from MK into the sinusoid (endothelia in red) in a FLK-1-EGFP Tg mouse immunostained with GP1b β . (ii) SEM image of a typical proplatelet with a smooth surface in the sinusoid. (iii) Magnified optical section of inset in Fig.5C-i. GPIb β expression is positive on the outer surface of the proplatelet. (iv) TEM image of proplatelet with a balloon-like swelling at its apical end. Both are devoid of PZ. (v) Magnified view of inset in (iv) depicting the specific granules and organelles of a proplatelet. The microtubules (red arrows) run longitudinally to the long axis of the proplatelet. Scale bar: 5 μm in (i), 1 μm in (ii,iii), 10 μm in (iv), 500 nm in (v). **(D) Proplatelet (platelet progenitor) released into the sinusoid.** (i) TEM image of platelet progenitor. (ii) Magnified view of inset in (i). The microtubules (red arrows) run parallel to the long axis of the platelet progenitor to form the marginal band of platelet. (iii) SEM image of platelet progenitor in sinusoid. Scale bar: 1 μm in (i,iii), 500 μm in (ii). EC: endothelial cell. MK: megakaryocyte. PZ: peripheral zone. S: sinusoid. R: red blood cell.

Figure 6. Platelet, reticulated platelet, and thick protrusion fluctuations after phlebotomy (A) and administration of anti-platelet serum (B).

Black circles (●) and squares (■) indicate platelet and reticulated platelet numbers, respectively, in venous blood. White squares (□) represent the ratio (%) of thick protrusions in all intravascular protrusions from MKs in the BM. Intravascular protrusions were quantified and categorized based on their maximum width and staining pattern as probed with anti-GPIb antibody. The ratio of thick protrusion was remarkably high when the platelet number was below the normal range. Reticulated platelet number, representing newly generated platelets, also increased in that period, but promptly decreased as the platelet number recovered to the normal level. Experimental repeats ≥ 3 . Data are mean \pm SD.

Figure 7. Summarized schema representing our results for platelet formation from MKs via thick protrusion or proplatelet.

(Top) Thick protrusion from mature MK (characterized by NZ, IZ, and PZ) adopted nodular or segmented shapes and the platelet progenitor is released into the peripheral blood in giant platelet like-form (characterized by IZ and PZ). (Bottom) At the initial

phase, fully mature MK (characterized by NZ and IZ) penetrated and grew into the sinusoid. The apical swelling was stretched by the bloodstream into a transitional proplatelet that remained thick before elongating into a thin long proplatelet with a beaded appearance along its length. Finally, the proplatelet snapped at the distal region and was released as a short proplatelet fragment into the peripheral blood. The proplatelet lacked, or had scant PZ at all sequential phases. Preplatelets could convert reversibly into platelets in the blood stream, outside BM (pale orange box). The mechanism for converting giant platelets into preplatelets or platelets is unknown. The endothelia are in red, NZ in light blue, IZ (consisting of PT and DMS) in orange, inner PZ in light green, and outer PZ in green.

Figure 2

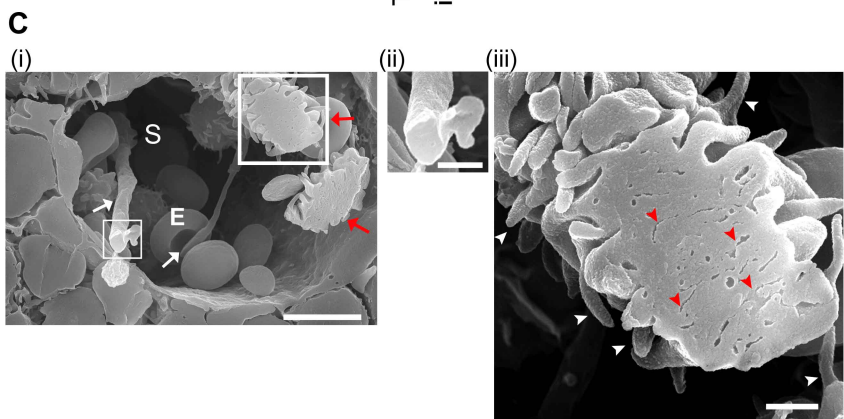
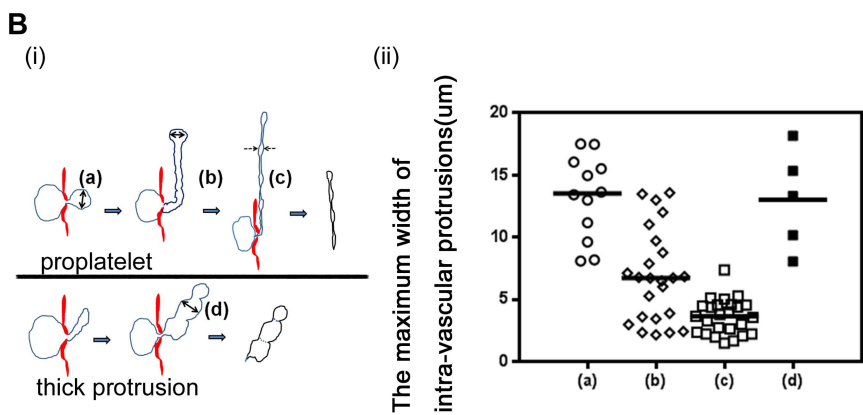
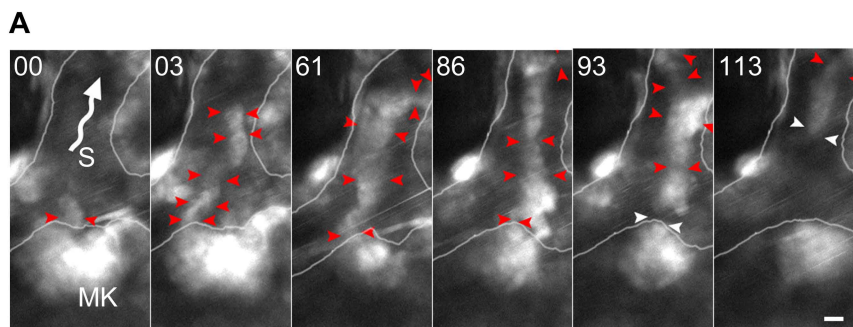


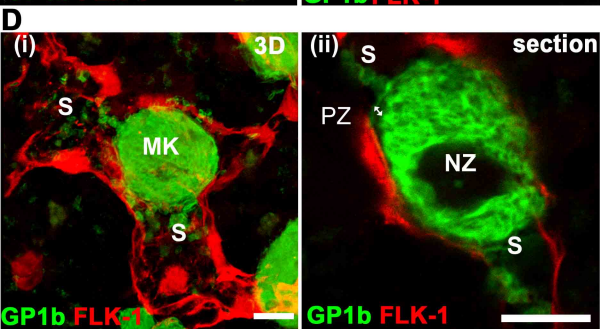
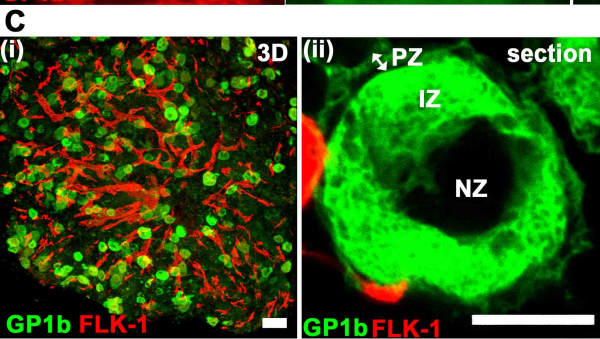
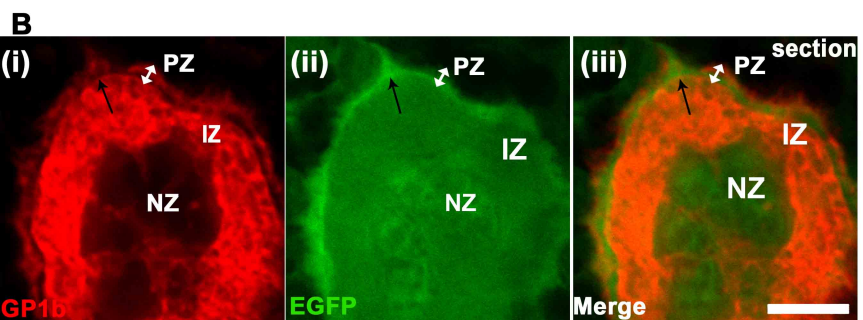
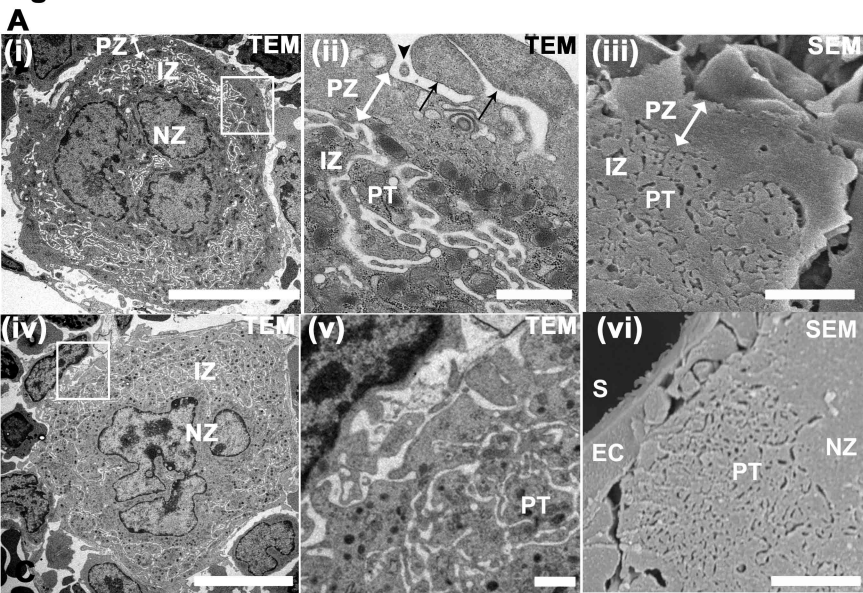
Figure 3

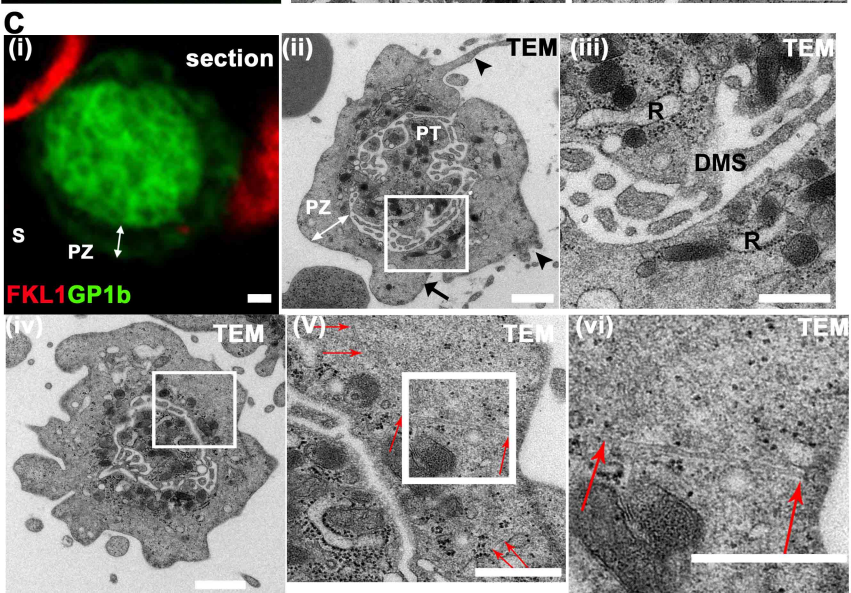
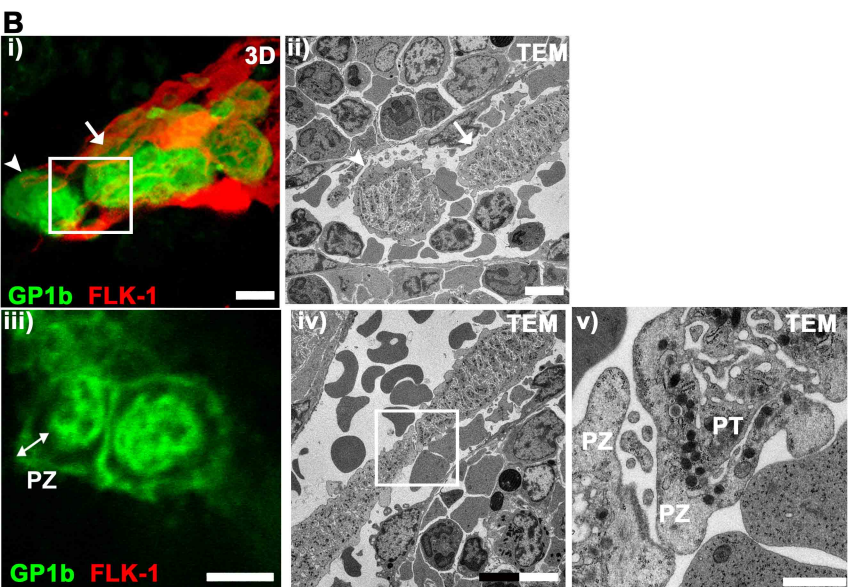
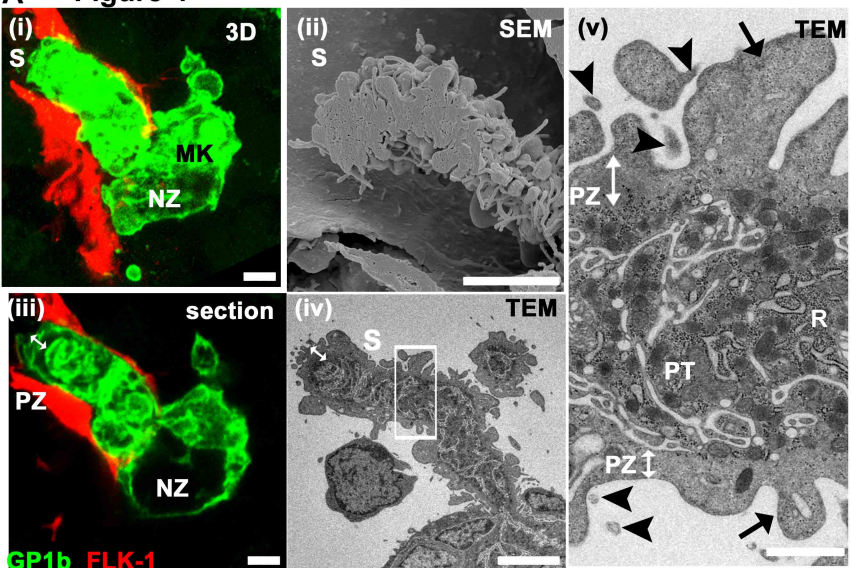
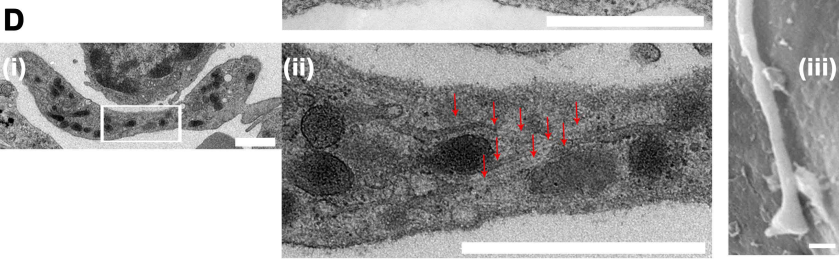
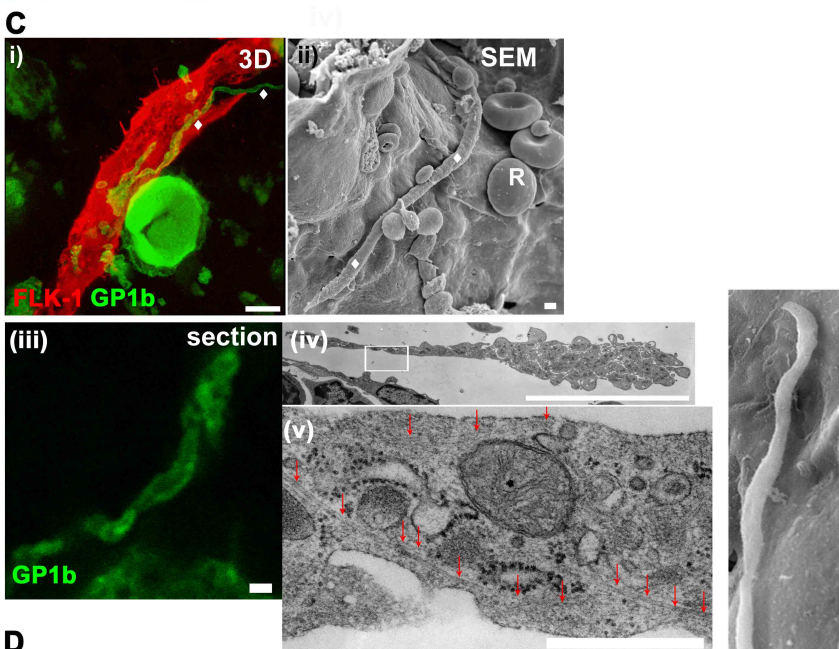
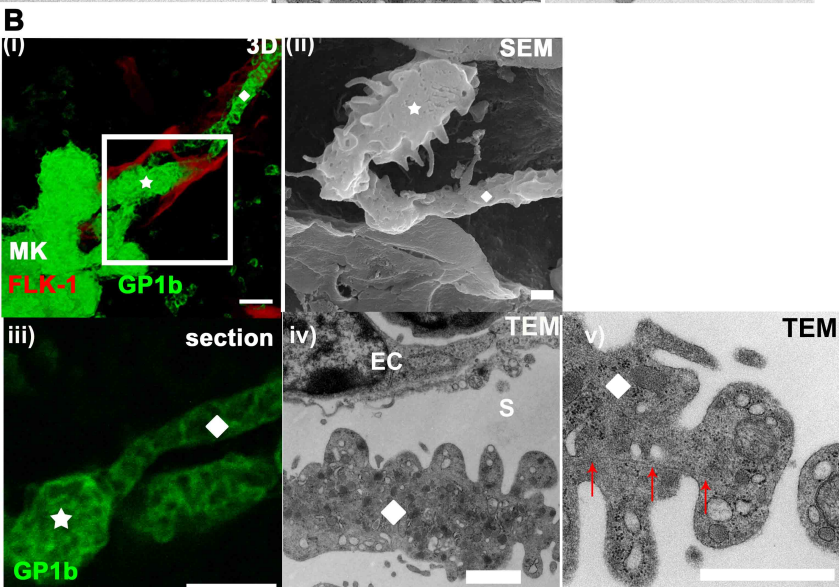
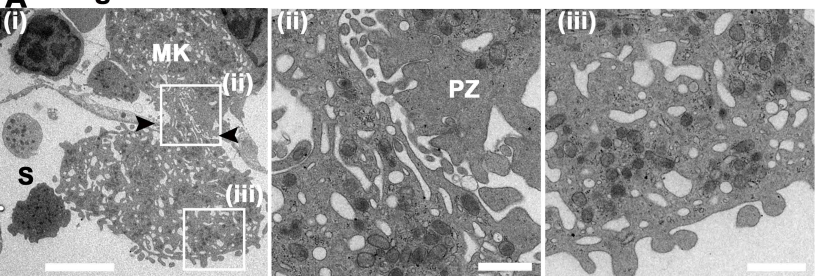
Figure 4

Figure 5

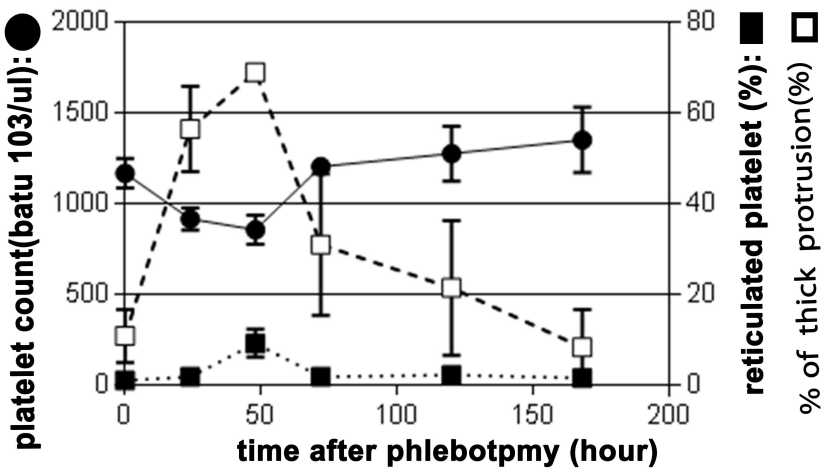
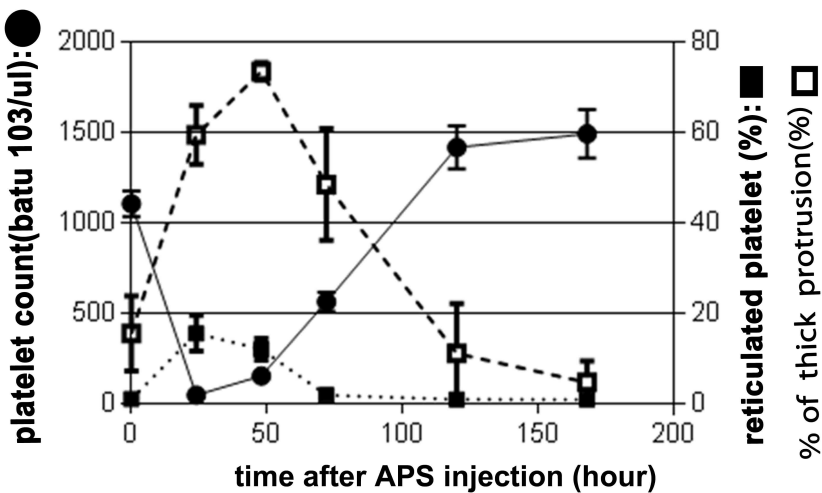
A**B**

Figure 7

